

Forschungszentrum Karlsruhe

Technik und Umwelt

Wissenschaftliche Berichte

FZKA 6501

The code CALUMO a tool for the analysis of
temperature transients in QUENCH tests

H. Steiner, M. Heck

Institut für Materialforschung

Projekt Nukleare Sicherheitsforschung

Zusammenfassung

CALUMO ein Rechencode für die Analyse von Temperaturtransienten in Abschreckversuchen

Der Code CALUMO wurde entwickelt, um Temperaturtransienten in FZK-Abschreckversuchen zu analysieren. Er basiert auf der Anwendung von Bilanzgleichungen für die Enthalpie der Brennstäbe, des Shrouds und des Kühlmittels. Es wird aber auch die Bildung der Oxidschichten auf den beteiligten Materialien berechnet. Ebenso wird eine Massenbilanz zwischen verbrauchtem Wasserdampf, aufgenommenem Sauerstoff und der Wasserstoffproduktion durchgeführt. Erste Rechnungen für QUENCH-03 und QUENCH-04 brachten sehr ermutigende Ergebnisse.

Abstract

The code CALUMO a tool for the analysis of temperature transients in QUENCH tests

The code CALUMO has been developed as a tool for the analysis of temperature transients in FZK QUENCH tests. This code is based on lumped parameter equations for the enthalpy of the fuel rods, the shroud, and the coolant. The code calculates also the evolution of oxide scales and establishes the mass balance on the consumed steam flow, the absorbed oxygen and the produced hydrogen. Scoping calculations for QUENCH-03 and QUENCH-04 provided very encouraging results.

CONTENTS

1.	Introduction.....	1
2.	Motivation for the development of the bundle code CALUMO.....	1
3.	Model development	1
	a) Radiative heat exchange between fuel rod simulators and shroud.	2
	b) Oxidation of fuel rod claddings and shroud.....	4
	c) Convective heat exchange between coolant and structural components	4
	d) Release of electrical power.....	7
	e) Axial heat conduction in the fuel rods and the shroud.....	7
	f) Heat losses	8
	g) Hydrogen generation	8
	h) Oxygen diffusion model.....	8
4.	Solution procedures.....	11
5.	Material data.....	13
6.	Initial conditions.....	15
7.	Results of scoping calculations for QUENCH-03 and QUENCH-04	16
8.	Conclusion.....	24
	References	24
	Annex I	25
	Annex II	28

1. Introduction

Temperature escalations are important phenomena in QUENCH tests as they lead to enhanced oxidation and hydrogen production and eventually to severe degradation in fuel rod bundles and maybe even blockage formation. Also, the state of the bundle at the end of the transient phase is seen to be very important for the events during the proper quench phase. Thus, the occurrence of unexpected temperature escalations in some quench tests of the CORA program [1] was a strong motive for the initiation of a new out-of-pile QUENCH Test Program at FZK with small bundles of electrically heated fuel rod simulators [2]. With five tests having been done in the meantime, an investigation of the outcome of these tests with regard to temperature escalation mechanisms might be helpful. Work has been started with a recalculation of the temperature transients in the QUENCH-03 and QUENCH-04 tests with the help of the computer code CALUMO, which has recently been developed.

2. Motivation for the development of the bundle code CALUMO

There are two elements from the experimental side which might help us to gain an understanding on what is happening during a quench test, namely the results of the test instrumentation like thermocouple readings and the outcome of post test examinations (PTE). PTE may provide us valuable hints on the mechanisms which were at work during a quench test. But, of course, they give us only a picture of the end of life state and the link to the bundle behavior at earlier time might not always be established in a clear-cut way.

Thus, it is indispensable to gain a quantitative understanding of the results of the test instrumentation, especially of the thermocouple readings. In order to achieve this, appropriate bundle codes have to be used.

Although there are at least half a dozen computer codes active in the light water reactor safety business, it was felt that a simple fast running bundle code might be of value on its own right. With such a code it would be much easier to test different oxide correlations and mechanisms.

A study of thermocouple readings of FZK quench tests reveals that in most cases the radial temperature profiles in the test bundles are rather flat. Thus, effects of thermal conductivity are not very important. Of course, there are exceptions from this rule, especially when severe azimuthal temperature gradients arise. But in these cases existing computer codes have also big problems to deal with such situations. When effects of thermal conductivity are not very important one can operate with lumped parameter models, that means balance equations. In this way modeling of bundle behavior simplifies considerably.

This idea was closely followed in developing the code CALUMO (**ca**lculations of temperature escalations in quench tests with the help of **l**umped parameter **m**odels). The calculation of the temperature evolution is based on three balance equations for the fuel rod simulators, the shroud, and the Ar/steam fluid.

3. Model development

As already mentioned in the foregoing section temperature calculations are based on three balance equations. They are given as follows:

i) for the fuel rod simulators:

$$\left[c_p^{cl} \cdot m^{cl} + c_p^{ox} \cdot m^{ox} + c_p^{el} \cdot m^{el} \right] \cdot \frac{dT_{rod}}{dt} = w^{el} + w_{cl}^{ox} - w_{rod}^{rad} - w_{cl}^{cool} + w_{rod}^{ax} \quad (1)$$

ii) for the shroud:

$$c_p^{\text{sh}} \cdot m^{\text{sh}} \frac{dT^{\text{sh}}}{dt} = w_{\text{sh}}^{\text{ox}} + w_{\text{sh}}^{\text{rad}} + w_{\text{sh}}^{\text{ax}} - w_{\text{sh}}^{\text{cool}} - w_{\text{sh}}^{\text{loss}} \quad (2)$$

iii) for the coolant:

$$\left(\dot{m}_{\text{Ar}} \cdot c_p^{\text{Ar}} + \dot{m}_{\text{st}} \cdot c_p^{\text{st}} \right) \frac{dT^{\text{cool}}}{dz} = w_{\text{cl}}^{\text{cool}} + w_{\text{sh}}^{\text{cool}} \quad (3)$$

Thus, the following mechanisms are taken into account:

- 1) Release of a electrical power in the fuel rod simulators
- 2) Radiative heat exchange between fuel rod simulators and the shroud
- 3) Convective heat exchange between the fuel rod simulators and the shroud on one hand and the coolant on the other hand
- 4) Release of heat due to oxidation of the fuel rod simulators and the shroud
- 5) Heat conduction through the ZrO₂ fiber insulation or Ar gap
- 6) Axial heat conduction in the fuel rod simulators and the shroud

It is also understood that the cladding mass m^{cl} and the shroud mass m^{sh} consist of an oxide and metallic part:

$$m^{\text{cl}} = m_{\text{ox}}^{\text{cl}} + m_y^{\text{cl}} \quad (4)$$

$$m^{\text{sh}} = m_{\text{ox}}^{\text{sh}} + m_y^{\text{sh}} \quad (5)$$

No modeling of mechanics is included within the frame of the CALUMO code. In this respect, the most important point would be the mechanical behavior of oxide scales. But at the moment we have no reliable creep correlation of oxide scales on Zry claddings, especially with regard to substoichiometry. Also, one important source of stresses are thermal gradients, which have been excluded due to the basic requirements of our model.

Consequences of mechanics on oxide scales like cracking and spalling could, of course, be dealt with in some approximate manner if this should reveal as necessary.

a) Radiative heat exchange between fuel rod simulators and shroud.

For the radiative heat exchange between the fuel rod simulators and the shroud mostly the outer row of fuel rods are responsible. As there is always some temperature profile over the fuel rod bundle, the outer fuel rods have in general temperatures lower than the average. As a rough approximation for this temperature effect we assume that the heat transfer and heat conduction effects in radial direction can be simulated by an effective thermal conductivity λ^{eff} . The radial temperature profile over the bundle is then given by:

$$T(r) = T^c - \frac{q}{4\lambda^{\text{eff}}} \cdot r^2 \quad (6)$$

with T^c the center temperature and q being the heat source density. The temperature difference over the bundle is:

$$\Delta T = \frac{q}{4\lambda^{\text{eff}}} \cdot (r_{\text{sh}}^i)^2 \quad (7)$$

$$q \cdot (r_{\text{sh}}^i)^2 = w^{\text{el}} + w_{\text{cl}}^{\text{ox}} \quad (8)$$

and

$$T^c = T^{\text{rod}} + \frac{1}{2}\Delta T \quad (9)$$

$$T_{\text{sur}} = T^{\text{rod}} - \frac{1}{2}\Delta T \quad (10)$$

In this way, effects of heat transfer and heat conductance can be roughly taken into account. Thus, the radiation heat transfer is given as:

$$w^{\text{rad}} = F(\varepsilon) \cdot \sigma \cdot (T_{\text{sur}}^4 - T_{\text{sh}}^4) \quad (11)$$

It is also assumed that:

$$w_{\text{rod}}^{\text{rad}} = w_{\text{sh}}^{\text{rad}} \quad (12)$$

that is, no radiation heat is absorbed by the coolant.

σ = Stefan-Boltzmann constant

$F(\varepsilon)$ = emissivity factor

$$F(\varepsilon) = \left[\frac{1}{\varepsilon_{\text{cl}}} + \frac{r_b^o}{r_{\text{sh}}^i} \left(\frac{1}{\varepsilon_{\text{sh}}} - 1 \right) \right]^{-1} \quad (13)$$

The effective outer radius r_b^o of the bundle is somewhat smaller than the inner radius of the shroud r_{sh}^i . But as it would be cumbersome to calculate the exact value, it is assumed that:

$$r_b^o \approx r_{\text{sh}}^i$$

Generally, the claddings and the inner surface of the shroud are oxidized. Therefore it is set:

$$\varepsilon_{\text{cl}} = \varepsilon_{\text{sh}} = \varepsilon_{\text{ox}} = 0,8$$

b) Oxidation of fuel rod claddings and shroud

In order to calculate the power released by the oxidation of the claddings w_{cl}^{ox} and the shroud w_{sh}^{ox} one needs the respective oxygen currents j^{ox} . For this we use the physically meaningful correlation:

$$j^{ox} = \frac{k(T)}{\delta^{ox}} \quad (14)$$

with δ^{ox} supplied by an experimental correlation. As we have non-isothermal temperature conditions, the evolution of the oxide scales is calculated according to:

$$\delta^{ox}(t + \Delta t) = \sqrt{\delta^{ox}(t)^2 + a(t)^2 \cdot \Delta t} \quad (15)$$

Thus, w_{cl}^{ox} and w_{sh}^{ox} are given as follows:

$$w_{cl}^{ox} = \Delta H^{ox} \cdot (u_{cl}^o \cdot j_{cl}^{ox}(T_{sur}) + u_{cl}^i \cdot j_{cl}^{ox}(T^c)) \quad (16)$$

$$w_{sh}^{ox} = \Delta H^{ox} \cdot (u_{sh}^i \cdot j_{sh}^{ox}(T^{sh})) \quad (17)$$

$$\Delta H^{ox} = 19,06 \cdot 10^3 \text{ J/g} \quad (18)$$

u_{cl}^o = total circumference of the outer fuel rod simulators

u_{cl}^i = total circumference of the inner fuel rod simulators

$u_{sh}^i = 2\pi \cdot r_{sh}^i$ = inner circumference of the shroud (19)

Thus, it is assumed that there is no oxidation at the inside of the claddings and at the outside of the shroud. But it would, in principle, not be difficult to allow for such processes. This would only mean some redefinition of the u parameters.

The uptake of oxygen by the claddings and the shroud, spacers and thermocouples leads to a reduction of the steam mass flow. For an axial section Δz this is calculated as:

$$\dot{m}^{st}(z + \Delta z) = \dot{m}^{st}(z) - \Delta z \cdot (u_{cl}^o \cdot j_{cl}^{ox}(T_{sur}) + u_{cl}^i \cdot j_{cl}^{ox}(T^c) + u_{sh}^i \cdot j_{sh}^{ox}(T^{sh})) \quad (20)$$

c) Convective heat exchange between coolant and structural components

The two contributions w_{cl}^{cool} and w_{sh}^{cool} are given as follows:

$$w_{cl}^{cool} = u_{cl} \cdot h_{sc} \cdot (T^{rod} - T^{cool}) \quad (21)$$

and

$$w_{sh}^{cool} = u_{sh}^i \cdot h_{sc} \cdot (T^{sh} - T^{cool}) \quad (22)$$

$$u_{cl} = u_{cl}^o + u_{cl}^i$$

The convective heat transfer coefficient is calculated via the following correlation for the Nusselt number [3]:

$$Nu = 0,021 \cdot Re^{0,8} \cdot Pr^{0,6} \cdot \left(\frac{T^{cool}}{T^{rod}} \right)^{0,575} \quad (23)$$

$$h_{sc} = \frac{Nu \cdot \lambda^{cool}}{d_{hyd}} \quad (24)$$

The Reynolds and Prandl numbers of the coolant are given as:

$$Re = \frac{\rho^{cool} \cdot d_{hyd} \cdot v^{cool}}{\mu^{cool}} \quad (25)$$

$$Pr = \frac{\mu^{cool} \cdot c_p^{cool}}{\lambda^{cool}} \quad (26)$$

The specific density of the coolant is calculated with the help of the general gas equation:

$$\frac{p}{\rho^{cool}} = \frac{T^{cool}}{R} \cdot \frac{v_{Ar} + v_{st}}{M_{Ar} \cdot v_{Ar} + M_{st} \cdot v_{st}} \quad (27)$$

$$v_{Ar} = \frac{\dot{m}_{Ar}}{M_{Ar}} \quad (28)$$

$$v_{st} = \frac{\dot{m}_{st}}{M_{st}} \quad (29)$$

M_{Ar} = molecular weight of Ar

M_{st} = molecular weight of steam

R = gas constant

The coolant velocity is then given by:

$$v^{\text{cool}} = \frac{\dot{m}}{\rho^{\text{cool}} \cdot F^{\text{cool}}} \quad (30)$$

F^{cool} = overall cross section of the coolant channel.

The hydraulic diameter is then calculated with the help of:

$$d_{\text{hyd}} = \sqrt{\frac{4F^{\text{rod}}}{\pi}} \quad (31)$$

$$F^{\text{rod}} = \frac{F^{\text{cool}}}{N^{\text{rod}}} \quad (32)$$

N^{rod} = number of fuel rod simulators

In order to calculate the material parameters of the Ar/steam coolant the model of Wilke [4] for binary gas mixtures is used.

$$\eta^{\text{cool}} = \frac{y_{\text{st}} \cdot \eta_{\text{st}}}{y_{\text{st}} + y_{\text{Ar}} \cdot \phi_{12}} + \frac{y_{\text{Ar}} \cdot \eta_{\text{Ar}}}{y_{\text{Ar}} + y_{\text{st}} \cdot \phi_{21}} \quad (33)$$

$$\phi_{12} = \frac{\left[1 + \left(\frac{\eta_{\text{st}}}{\eta_{\text{Ar}}} \right)^{\frac{1}{2}} \cdot \left(\frac{M_{\text{Ar}}}{M_{\text{st}}} \right)^{\frac{1}{4}} \right]^2}{\left[8 \left(1 + \frac{M_{\text{st}}}{M_{\text{Ar}}} \right) \right]^{\frac{1}{2}}} \quad (34)$$

$$\phi_{21} = \phi_{12} \cdot \frac{\eta_{\text{Ar}}}{\eta_{\text{st}}} \cdot \frac{M_{\text{st}}}{M_{\text{Ar}}} \quad (35)$$

with $y_{\text{st}} = \frac{v_{\text{st}}}{v_{\text{st}} + v_{\text{Ar}}} \quad (36)$

$$y_{\text{Ar}} = \frac{v_{\text{Ar}}}{v_{\text{st}} + v_{\text{Ar}}} \quad (37)$$

For λ^{cool} a formula similar to (33) is used with λ_{st} and λ_{Ar} replacing η_{st} and η_{Ar} .

d) Release of electrical power

The release of electrical power is done via Ohm heating. Thus, the release of electrical power in a certain axial section is proportional to its electrical resistance. The overall electrical resistance is given by:

$$R^{tot} = R^{in} + R_{cu}^u + R_{cu}^l + R_{Mo}^u + R_{Mo}^l + R_W \quad (38)$$

With R^{in} the resistance of the sliding contacts, screws, wires and so on. This parameter has not been measured.

In general, we have axial temperature distributions in the different electrodes. Therefore their resistances are calculated as follows:

$$R_{el} = \frac{\sum}{k} \cdot \frac{\Delta z_k}{F_{el}} \cdot r_{el}(T_k) \quad (39)$$

Thus, the electric power released in a certain electrode is given by:

$$P_{el} = \frac{R_{el}}{R^{tot}} \cdot P^{tot} \quad (40)$$

and the linear power at a certain axial position z:

$$\chi_{el} = \frac{P_{el}}{R_{el}} \cdot \frac{r_{el}(T(z))}{F_{el}} \quad (41)$$

e) Axial heat conduction in the fuel rods and the shroud

The thermal conductivity of the electrodes is rather high. Therefore the effect of axial heat conduction has to be taken into account. This effect might be relevant for the specific conditions of the FZK quench tests, but less in the reactor case. Although there is also some axial heat conduction in Zry components.

The contributions w_{rod}^{ax} and w_{sh}^{ax} are given as follows:

$$w_{rod}^{ax} = (\lambda_y \cdot F_y^{cl} + \lambda_{el} \cdot F_{el}) \cdot \frac{\partial^2 T^{rod}}{\partial z^2} \quad (42)$$

$$w_{sh}^{ax} = \lambda_y \cdot F_y^{sh} \cdot \frac{\partial^2 T^{sh}}{\partial z^2} \quad (43)$$

f) Heat losses

The thermal shield of the test section consists of a 35 mm thick ZrO₂ fiber insulation along the heated zone between 0 and about 1024 mm axial position. Above the 1024 mm elevation there is an Ar gap between the shroud and the annular cooling jacket. The heat losses are then given by:

$$W_{ZrO_2}^{loss} = \frac{(T^{sh} - T_i^{cj})}{\ln \cdot \frac{r_i^{cj}}{r_o^{sh}}} \cdot 2\pi\lambda^{iso} \quad (44)$$

and

$$W_{Ar}^{loss} = \frac{(T^{sh} - T_i^{cj})}{\ln \frac{r_i^{cj}}{r_o^{sh}}} \cdot 2\pi\lambda^{Ar} + F(\varepsilon) \cdot \sigma \cdot (T^{sh4} - T_i^{cj4}) \quad (45)$$

g) Hydrogen generation

The hydrogen flux can be easily obtained from the oxygen flux:

$$j^H = \frac{1}{8} \cdot j^{ox} \quad (46)$$

Thus, the amount of hydrogen produced during a time increment Δt over an axial length Δz is given by:

$$\Delta(\Delta m^H) = \frac{1}{8} \cdot \left[(u_{cl}^o \cdot j_{cl}^{ox}(T_{sur}) + u_{cl}^i \cdot j_{cl}^{ox}(T^c) + u_{sh}^i \cdot j_{sh}^{ox}(T^{sh}) \right] \cdot \Delta t \cdot \Delta z \quad (47)$$

In order to obtain the total amount of hydrogen produced during the time interval Δt one has to sum up over all the axial increments Δz :

$$\Delta m^H = \sum_{all \Delta z} \Delta(\Delta m^H) \quad (48)$$

The hydrogen production rate is then given by:

$$\dot{m}^H = \frac{\Delta m^H}{\Delta t} \quad (49)$$

h) Oxygen diffusion model

In a special version of the code (CALUMO-D) a model for the calculation of oxygen diffusion in the claddings and the shroud is implemented. This model replaces then the data correlations on oxide scale thickness and oxygen fluxes.

The oxygen diffusion model implemented in CALUMO-D is based on the work of Moalam and Olander [5]. These authors applied a special procedure to solve the diffusion equation. With regard to the radial position simple functions are assumed. This leads to differential equations for the time dependent parameters of these functions, whose solution is much easier than that of the diffusion equation. For more information on this method the reader is referred to ref. [5].

For our purposes the treatment of stage 4 as defined in [5] is sufficient (fixed oxygen concentration at the surface). The approximate distribution of oxygen in the oxide scale is:

$$C_o^{ox} = C_{os} - (C_{os} - C_{ox}) \cdot \frac{x}{\delta^{ox}} - S_o \cdot \frac{x}{\delta^{ox}} \cdot \left(1 - \frac{x}{\delta^{ox}}\right) \quad (50)$$

x = distance from the surface

In the α -phase the oxygen distribution is put in the same way:

$$C_\alpha^{ox} = C_{\alpha\omega} - (C_{\alpha\omega} - C_{\alpha\beta}) \cdot \phi_\alpha - S_\alpha \cdot \phi_\alpha (1 - \phi_\alpha) \quad (51)$$

with

$$\phi_\alpha = \frac{x - \delta^{ox}}{\delta^\alpha} \quad (52)$$

and in the β -phase the following ansatz is used:

$$C_\beta^{ox} = C_{\beta\alpha} (1 - \phi_\beta)^n + S_\beta [1 - (1 - \phi_\beta)^n] \quad (53)$$

with:

$$\phi_\beta = \frac{x - (\delta^{ox} + \delta^\alpha)}{\delta^\beta} \quad (54)$$

The parameters S_o , S_α and S_β are calculated with the help of the following differential equations:

$$\dot{S}_o = \frac{12D^{ox} \cdot S_o}{(\delta^{ox})^2} + \frac{\dot{\delta}^{ox}}{\delta^{ox}} [3(C_{os} - C_{o\alpha}) - S_o] \quad (55)$$

$$\dot{\delta}^{ox} = \frac{\frac{D^{ox}}{\delta^{ox}} [C_{os} - C_{o\alpha} - S_o] - \frac{D^\alpha}{\delta^\alpha} [C_{\alpha\omega} - C_{\alpha\beta} + S_\alpha]}{C_{o\alpha} - \frac{C_{\alpha\omega}}{PB}} \quad (56)$$

$$\frac{n}{n+1} \cdot \frac{x_{\max} - x_{\alpha\beta}}{C_{\beta\alpha} - S_\beta} \cdot S_\beta = \frac{n \cdot D^\beta}{x_{\max} - x_{\alpha\beta}} + \frac{PB-1}{PB} \cdot \left(1 - \frac{\dot{\delta}^{ox}}{n+1}\right) - \frac{n}{n+1} \cdot \dot{x}_{\alpha\beta} \quad (57)$$

$$\dot{x}_{\alpha\beta} = \frac{PB-1}{PB} \cdot \dot{\delta}^{\text{ox}} + \frac{\frac{D^\alpha}{\delta^\alpha} [C_{\alpha\omega} - C_\beta - S_\alpha] - \frac{nD^\beta \cdot (C_{\beta\alpha} - S_\beta)}{x_{\text{max}} - x_{\alpha\beta}}}{C_{\alpha\beta} - C_{\beta\alpha}} \quad (58)$$

$$\dot{S}_\alpha = \frac{12 \cdot D^\alpha \cdot S_\alpha}{(\delta^\alpha)^2} + \frac{3 \cdot \left(\dot{x}_{\alpha\beta} + \dot{\delta}^{\text{ox}} \right) \cdot (C_{\alpha\omega} - C_{\alpha\beta}) - (\dot{x}_{\alpha\beta} - \dot{\delta}^{\text{ox}}) S_\alpha}{\delta^\alpha} - 6 \cdot \frac{PB-1}{PB} \cdot \frac{(C_{\alpha\omega} - C_{\alpha\beta}) \cdot \dot{\delta}^{\text{ox}}}{\delta^\alpha} \quad (59)$$

PB = Pilling-Bedworth ratio (PB=1.56)

$C_{s\omega}, C_{d\alpha}$ = oxygen concentrations at the phase boundaries of the oxide phase

$C_{\alpha\omega}, C_{\alpha\beta}$ = oxygen concentrations at the phase boundaries of the α -phase

$C_{\beta\alpha}$ = oxygen concentrations at the phase boundaries of the β -phase

The differential equations (55) to (59) are solved with the help of finite difference schemes in a forward direction. Thus, the values of the oxide scale δ^{ox} and δ^α after a time increment Δt are calculated as follows:

$$\delta^{\text{ox}}(t + \Delta t) = \delta^{\text{ox}}(t) + \Delta t \cdot \dot{\delta}^{\text{ox}}(t) \quad (60)$$

and

$$\delta^\alpha(t + \Delta t) = \delta^\alpha(t) + \Delta t \cdot (\dot{x}_{\alpha\beta}(t) - \dot{\delta}^{\text{ox}}(t)) \quad (61)$$

The parameter x_{max} is the actual thickness of the cladding or the shroud:

$$x_{\text{max}} = S^{cl} + \frac{PB-1}{B} \cdot \delta^{\text{ox}} \quad (62)$$

If the temperature is below about 910 °C no β -phase is present. In this case we use the following distribution in the α -phase:

$$C_o^\alpha = C_{\alpha\omega} \cdot \exp\left(-\frac{x - \delta^{\text{ox}}}{p_\alpha}\right) \quad (63)$$

The parameter p_α is determined with the help of:

$$\dot{p}_\alpha = -\dot{\delta}^{\text{ox}} + \frac{D^\alpha}{p_\alpha} \quad (64)$$

For temperatures above about 910 °C the β -phase disappears when:

$$\delta^{\text{ox}} + \delta^\alpha \geq x_{\text{max}} \quad (65)$$

In this case, the following distribution is assumed in the α -phase:

$$C_o^\alpha = C_{\infty} (1 - \phi_\alpha)^n + S_\alpha \cdot [1 - (1 - \phi_\alpha)^n] \quad (66)$$

with:

$$\phi_\alpha = \frac{x - \delta^{\text{ox}}}{x_{\text{max}} - \delta^{\text{ox}}} \quad (67)$$

and S_α determined by:

$$\frac{n}{n+1} \cdot \frac{x_{\text{max}} - \delta^{\text{ox}}}{C_{\infty} - S_\alpha} \cdot \dot{S}_\alpha = \frac{n \cdot D^\alpha}{x_{\text{max}} - \delta^{\text{ox}}} - \frac{n}{n+1} \cdot \dot{\delta}^{\text{ox}} \quad (68)$$

According to [5], n is normally between 4 and 5. We have taken a fixed value of 4.5.

The oxygen flux entering the oxide phase is given by:

$$j^{\text{ox}} = \frac{D^{\text{ox}}}{\delta^{\text{ox}}} \cdot (C_{\text{so}} - C_{\text{o}\alpha} + S_o) \quad (69)$$

and the oxygen flux entering the metal phase:

$$j^{\text{me}} = \frac{D^\alpha}{\delta^\alpha} (C_{\infty} - C_{\alpha\beta} + S_\alpha) \quad (70)$$

Thus, the oxygen flux consumed in the oxide phase is given by:

$$j_r^{\text{ox}} = j^{\text{ox}} - j^{\text{me}} \quad (71)$$

The parameter j^{ox} is relevant for the calculation of oxygen uptake and hydrogen production and the parameter j_r^{ox} for the heat release due to the oxidation of the claddings and the shroud.

4. Solution procedures

The balance equations for the rod and shroud temperatures of the foregoing section are solved with the help of a Runge-Kutta integration procedure which could be found in textbooks on numerical mathematics (see for example [6]). The differential quotients $\frac{\delta T}{\delta z}$ and

$\frac{\delta^2 T}{\delta z^2}$ are approximated by the respective difference quotients:

$$\frac{\partial T}{\partial z} \approx \frac{T_{k+1} - T_k}{\Delta z} \quad (72)$$

$$\frac{\partial^2 T}{\partial z^2} \approx \frac{T_{k+1} + T_{k-1} - 2T_k}{\Delta z^2} \quad (73)$$

A detailed description of the test section is to be found for example in [7], a schematic view of the part relevant for the modeling is to be seen in Fig. 1. In the code CALUMO only the part between $z=0$ and $z=1300$ mm (upper end of cooling jacket) is modelled. In any case the temperatures in the lower part of the test section ($z<0$ mm) remain at low levels. Therefore this part does not much contribute to oxidation and hydrogen generation. Although it has some influence on the axial distribution of the electric power release.

The axial regions between 0 and 1024 mm and between 1024 and 1300 mm are each divided into equi-sized axial sections with length Δz_1 and Δz_2 in such a way that $\Delta z_1 \approx \Delta z_2$.

The temperatures T^{rod} and T^{sh} are calculated in the middle of each axial section, whereas the coolant temperature is calculated at the lower boundary of each section.

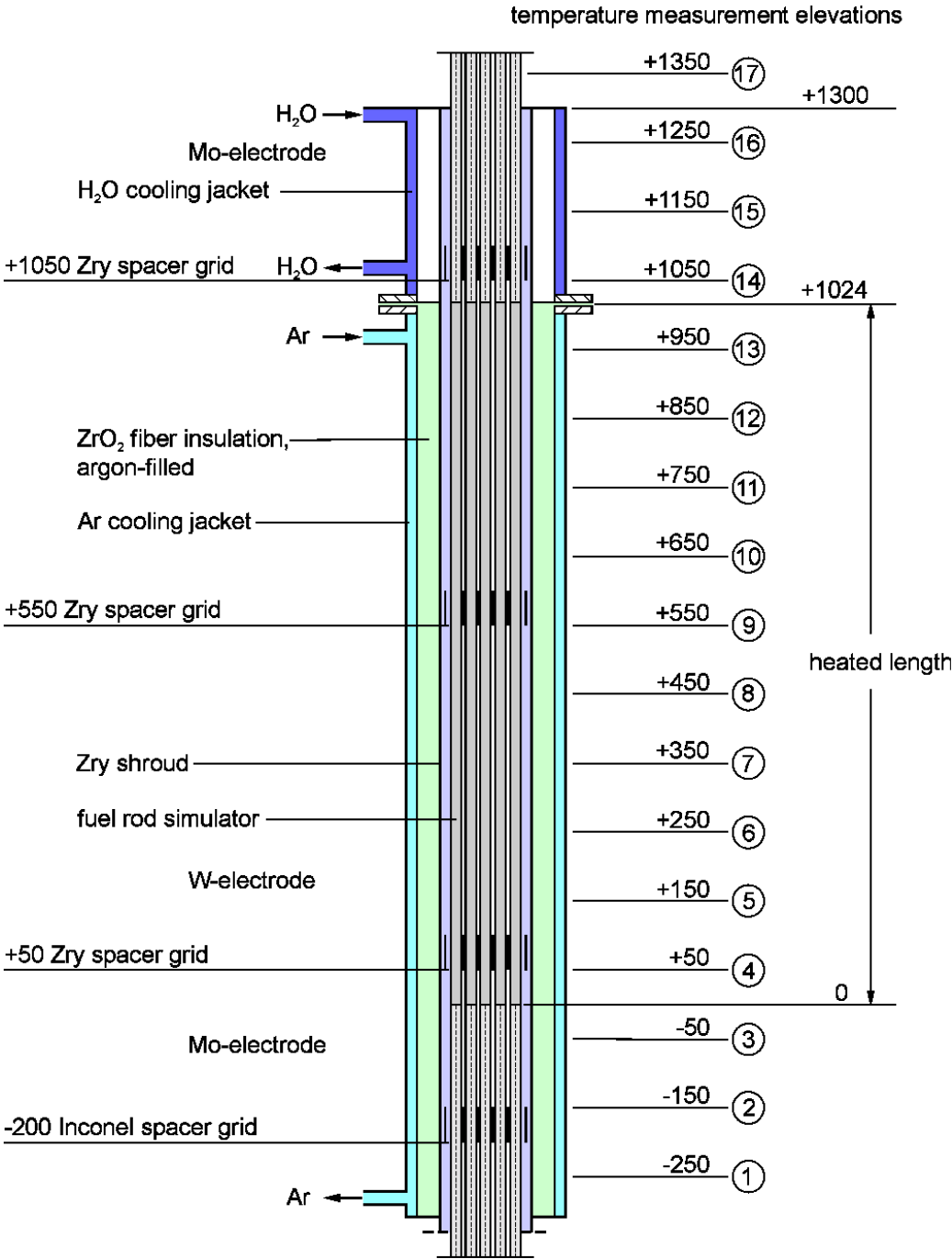


Fig. 1: Schematic view of the test section with the bundle

Therefore, in order to calculate the convective heat exchange in the k^{th} segment, one has to use:

$$T^{\text{cool}} = 0,5 \cdot (T_k^{\text{cool}} + T_{k+1}^{\text{cool}}) \quad (74)$$

as input for the equations (1) and (2) (see also Fig. 2).

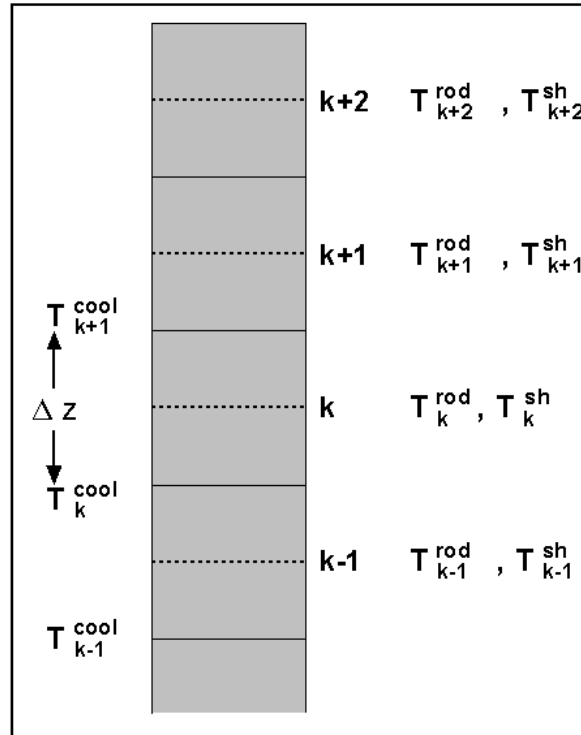


Fig. 2 Schematic view of the solution procedure for the coolant, rod, and shroud temperatures

5. Material data

A lot of material data correlations are needed in the computer code CALUMO. It would be too cumbersome to discuss them all. But for the information of the user of the code a list of the data correlations is included in the annex.

Of course, all these data correlations are necessary for the functioning of the code, but most of them have only a limited impact on the results. This is not true for the correlation on the oxide scale thickness δ^{ox} and the oxygen mass flux j^{ox} . They have indeed a decisive impact on the temperature evolution in the test bundle calculated by the code, and different data correlations can lead to very different results.

The main request, which should be fulfilled, is that both correlations are coherent. In the code CALUMO both correlations are coupled via:

$$j^{ox} = \frac{k(T)}{\delta^{ox}} \quad (75)$$

The parameter $k(T)$ is to be determined either by:

$$k(T) = D_{ox} \cdot \Delta C_{ox} \quad (76)$$

or by the use of a data correlation for j^{ox} :

$$k(T) = j^{ox} \cdot \delta^{ox} \quad (77)$$

In the future one of the main aims with the code CALUMO is to investigate the impact of different data correlations. But in the test phase of the code we stick to definite correlations.

Scoping calculations with the code have shown that with the following data correlations a reasonable agreement with the test results of QUENCH-03 could be obtained:

For $T \leq 1783$ K we have taken from [8]:

$$\delta^{ox} = 0,28 \cdot \exp(-10106/T) \cdot \sqrt{t} \quad (78)$$

and from [9]:

$$k(T) = D_{ox} \cdot \Delta C_{ox} = 0,098 \cdot \exp(-20373/T) \quad (79)$$

If one applies (76) to the correlations δ^{ox} and j^{ox} of [8] one would obtain:

$$k(T) = 0,1012 \cdot \exp(-20587/T) \quad (80)$$

For $T > 1783$ K we take the correlations of Prater/Courtright [10]:

$$\delta^{ox} = 5,46 \cdot \exp(-14120/T) \cdot \sqrt{t} \quad (81)$$

and

$$k(T) = j^{ox} \cdot \delta^{ox} = 15,67 \cdot \exp(-27430/T) \quad (82)$$

One has to note that in [8] and [10] correlations for the oxygen uptake are given. In order to obtain the oxygen current j^{ox} one has to differentiate these correlations with respect to the time t . This gives a factor of $\frac{1}{2}$.

6. Initial conditions

The code CALUMO is developed as a tool for the investigation of temperature escalations in FZK quench tests. Therefore it is not meant to simulate the conditions in the test bundles from the very beginning of the tests. But, of course, we need the conditions at the end of the steady-state phase in order to have the initial conditions for the calculations.

This is no problem for the clad and shroud temperatures, as there exist measured values. In the future one could even think of reading the respective values from the files of the tests. But at the moment a much simpler procedure is used. Namely, at $z=50$ and 950 mm we take the experimental values and for the values at the other axial locations we use linear interpolations or extrapolations. Thus for z_i between 0 and 1024 mm we have:

$$T(z_i) = T(z_{i-1}) + \Delta T^h \quad (83)$$

with

$$\Delta T^h = \frac{T(950) - T(50)}{LAX} \quad (84)$$

LAX = number of axial sections Δz on the heated section

and for z_i above 1024 mm.

$$T(z_i) = T(z_{i-1}) - \Delta T^{uh} \quad (85)$$

with ΔT^{uh} a suitable temperature increment in the unheated section.

The coolant temperatures are not measured. Therefore they must be calculated. In the steady-state conditions, the clad and shroud temperatures do not change with time. Thus, the electric power released in the bundle is used to heat-up the coolant. Also, the heat release due to oxidation is rather unimportant, as the temperatures are relatively low. Thus, the heat-up of the coolant is calculated as:

$$(\dot{m}_{Ar} \cdot C_p^{Ar} + \dot{m}_{st} \cdot C_p^{st}) \cdot \frac{dT^{cool}}{dz} = w^{el} - w^{loss} \quad (86)$$

In order to apply this equation we need the coolant temperature at $z=0$, the so called inlet temperature T_{in} . Unfortunately, the inlet temperature is measured at a much lower position and can therefore not be used. At the moment we use a value of 600 K for the inlet temperature and this is kept constant during the whole calculation.

7. Results of scoping calculations for QUENCH-03 and QUENCH-04

When the work for the development of CALUMO started, it was not really certain that such a simple model could provide a good simulation of the experimental results. This could only be checked with the help of validating calculations for different tests of the FZK quench program. In a first step, such calculations have been done for QUENCH-03 [11] and QUENCH-04 [12]. The results will be presented and discussed in the following.

The code CALUMO was developed for the analysis of temperature escalations. Thus, the calculation starts at the end of the steady state period of QUENCH-03 and QUENCH-04. Therefore for QUENCH-03 $t=0$ in the code corresponds to an experimental time of 900 s in [11] and the calculation ends just before the injection of the quench water, as there are no capabilities to treat the quench phase in the code. For QUENCH-04 the time $t=0$ in the code corresponds to an experimental time of 115 s (see also [12]) and the calculation goes far into the quench phase, as the capabilities of the code are sufficient to deal with steam quenching. The fit parameters, the empirical physical constants, the boundary, and the initial conditions used for the calculations are compiled in table 1 and 2. The same set of data was used for both tests.

Table 1: Correlation factors and empirical physical parameters used for the calculations of QUENCH-03 and QUENCH-04

Leistikow correlation	1.0
Prater/Courtright correlation	1.0
Convection heat transfer to the coolant	1.4
Axial heat transfer between W and Mo electrode at 1024 mm	0.05
Inlet electric resistance [m Ω]	4.2
Effective thermal conductivity over the bundle [W/cmK]	0.16

Table 2: Values of boundary conditions used for the calculations of QUENCH-03 and QUENCH-04

Fluid temperature at $z=0$ mm	600 K
Average bundle temperature below $z=0$ mm	800 K
Inner temperature of the stainless steel cooling jacket	400 K
Inner temperature of the H ₂ O cooling jacket	400 K
Average bundle temperature above $z=1350$ mm	600 K

The heated length of 1024 mm is subdivided into 20 axial segments, with the respective axial node point lying just in the middle of each axial segment. Thus, the respective node points are not directly at the locations of the thermocouples but some few millimeters off.

The strongest impact on the temperatures in the bundle comes from the choice of the oxidation correlations. In a first round of calculations we have taken for temperatures below 1783K the correlations of Leistikow and Veshchunov (see section 5) and for temperatures above 1783 K the correlations of Prater/Courtright. We have termed this our base case. But it became evident rather early that this choice of correlations did not provide a satisfying simulation of the experimental results. Therefore we have done a second round of calculations with the correlations of Leistikow/Veshchunov alone assumed to be valid over the whole temperature range. This we have termed the low oxidation case.

In Fig. 3 evolutions of the rod and shroud temperatures of QUENCH-03 for the base case are to be seen showing very high temperature increase rates at the end of the transient phase. This is not in accord with the experimental findings. Also, these high temperature increase rates can lead to numerical problems in the code in such a way that we come into a run-away situation. Therefore we have switched to the low oxidation case.

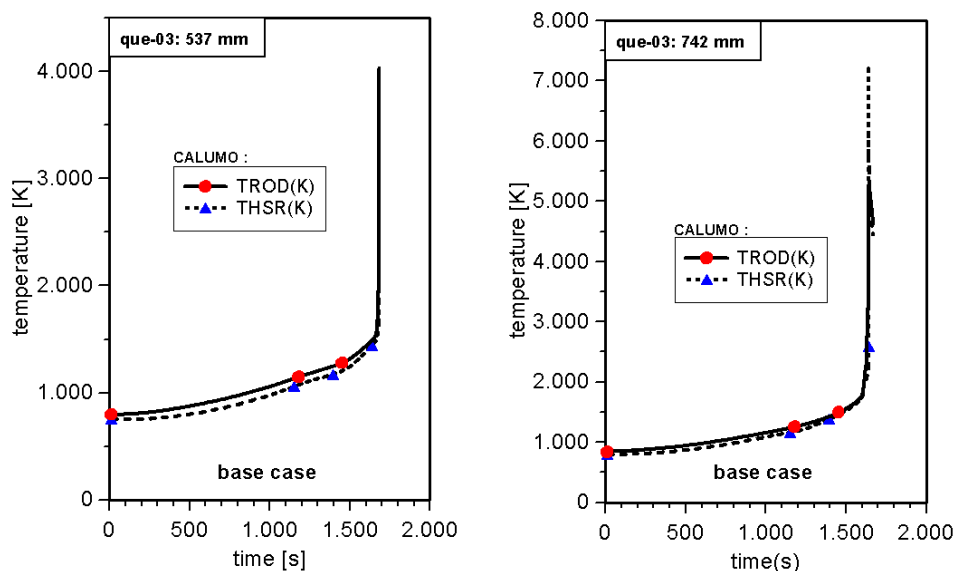


Fig. 3: Evolution of rod and shroud temperatures at 742.4 and 537.6 mm for the base case

In Fig. 4 to 10 results for QUENCH-03 are to be seen and in Fig. 11 to 16 results for QUENCH-04. For QUENCH-03 the calculated rod and shroud temperatures are in general rather near to the measured ones. The temperature escalation at 750 mm starting at about 1500 s into the transient is not reproduced by the code with the chosen set of parameters. This temperature escalation is presumably due to bending of the fuel leading to an impaired heat removal. This can be simulated by a strongly decreased effective thermal conductivity in the inner part of the bundle. In this way, a temperature escalation can also be obtained by the code (see Fig. 10). The temperature escalation in the upper part of the shroud, seen by the thermocouples, is not calculated by the code. This temperature escalation of the shroud is presumably due to natural convection in the Ar-volume around the shroud starting at a critical Grashof number [14]. This effect is not yet modeled in the code. It might be linked to a strong increase of the heat losses in the heated part of the test section.

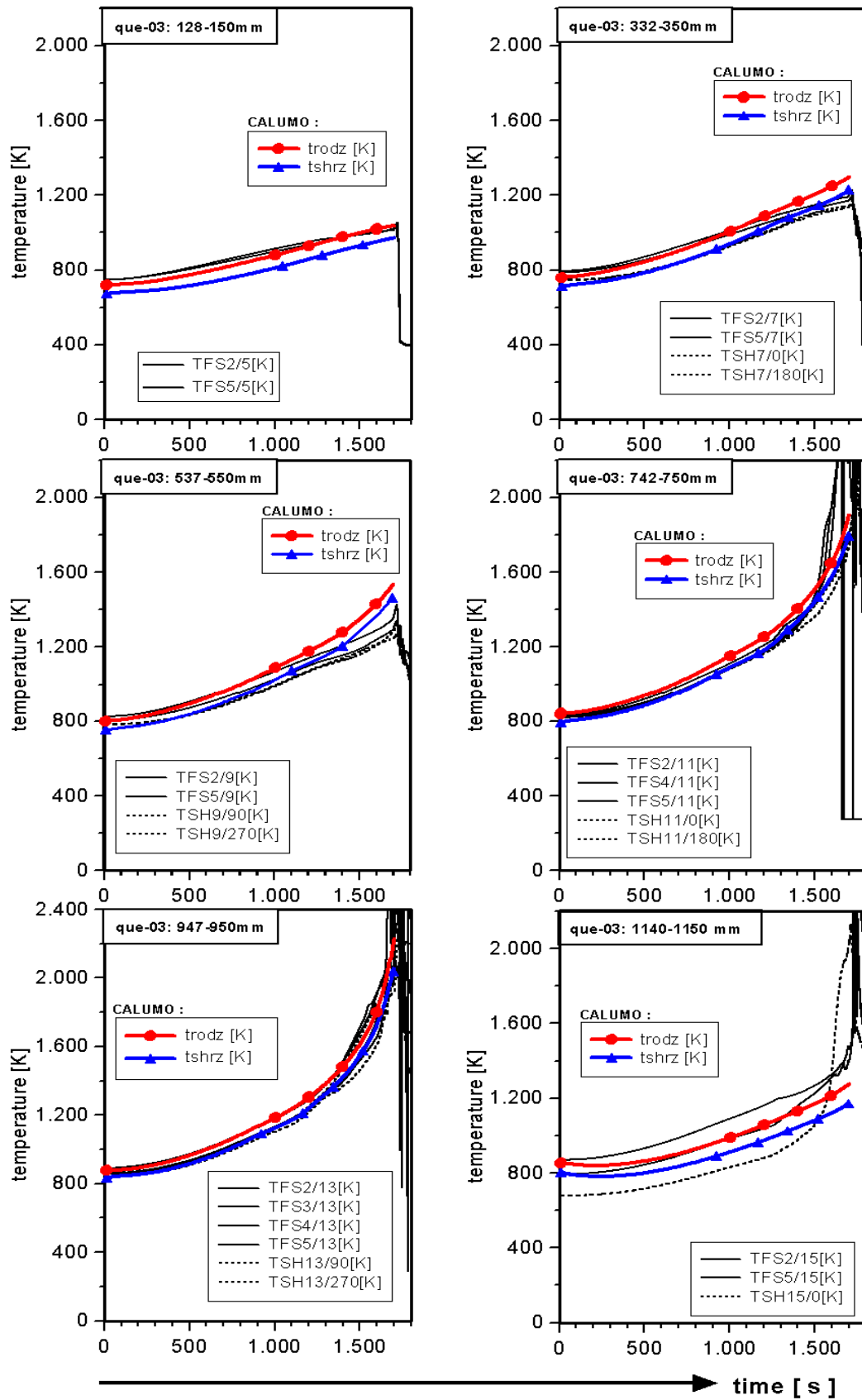


Fig. 4 Evolution of rod and shroud temperatures of QUENCH-3 at different axial locations (low ox. case)

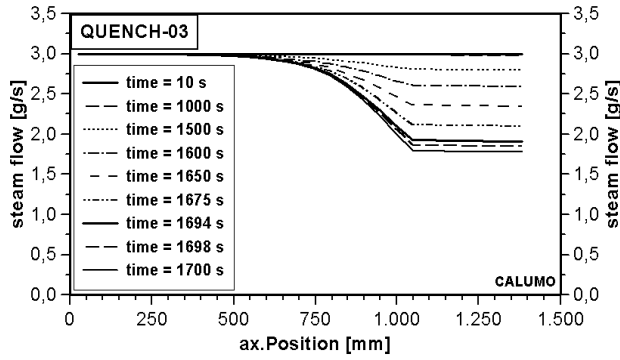


Fig. 5 Axial distributions of the steam flow rate at different times into the transient (low oxidation case)

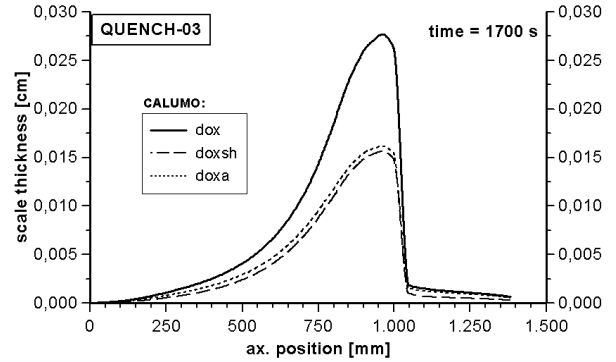


Fig. 6 Axial distributions of the oxide scale thickness at the end of the transient (low oxidation case)

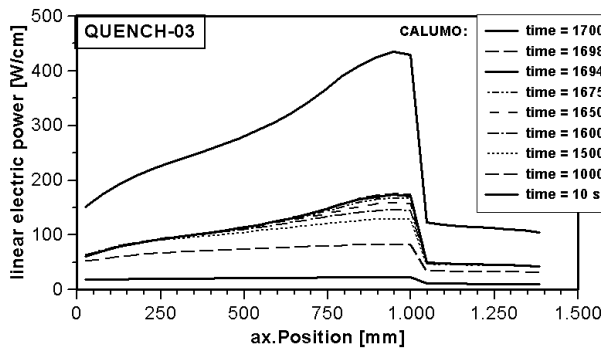


Fig. 7 Axial distributions of the linear electric power at different times into the transient (low oxidation case)

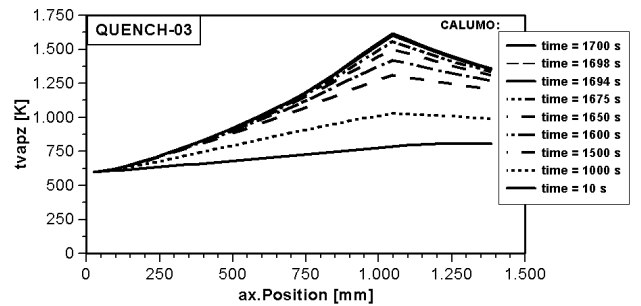


Fig. 8 Axial distributions of the coolant temperature at different times into the transient (low oxidation case)

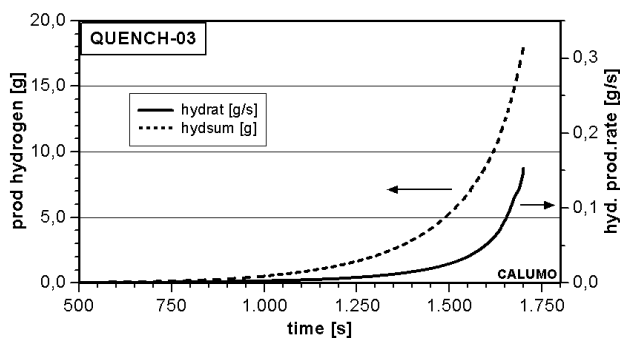


Fig. 9 Evolution of the hydrogen production rate and produced hydrogen during the transient phase of QUENCH-03 (low oxidation case)

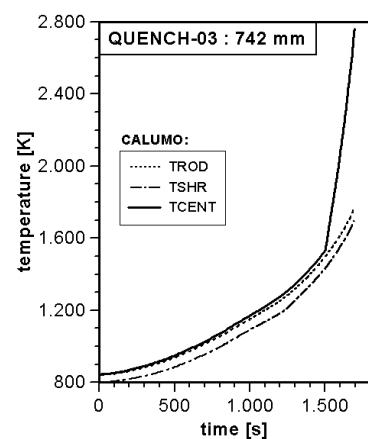


Fig. 10 Evolution of rod and shroud temperatures at about 750 mm for a reduced effective thermal conductivity in the inner part of the bundle

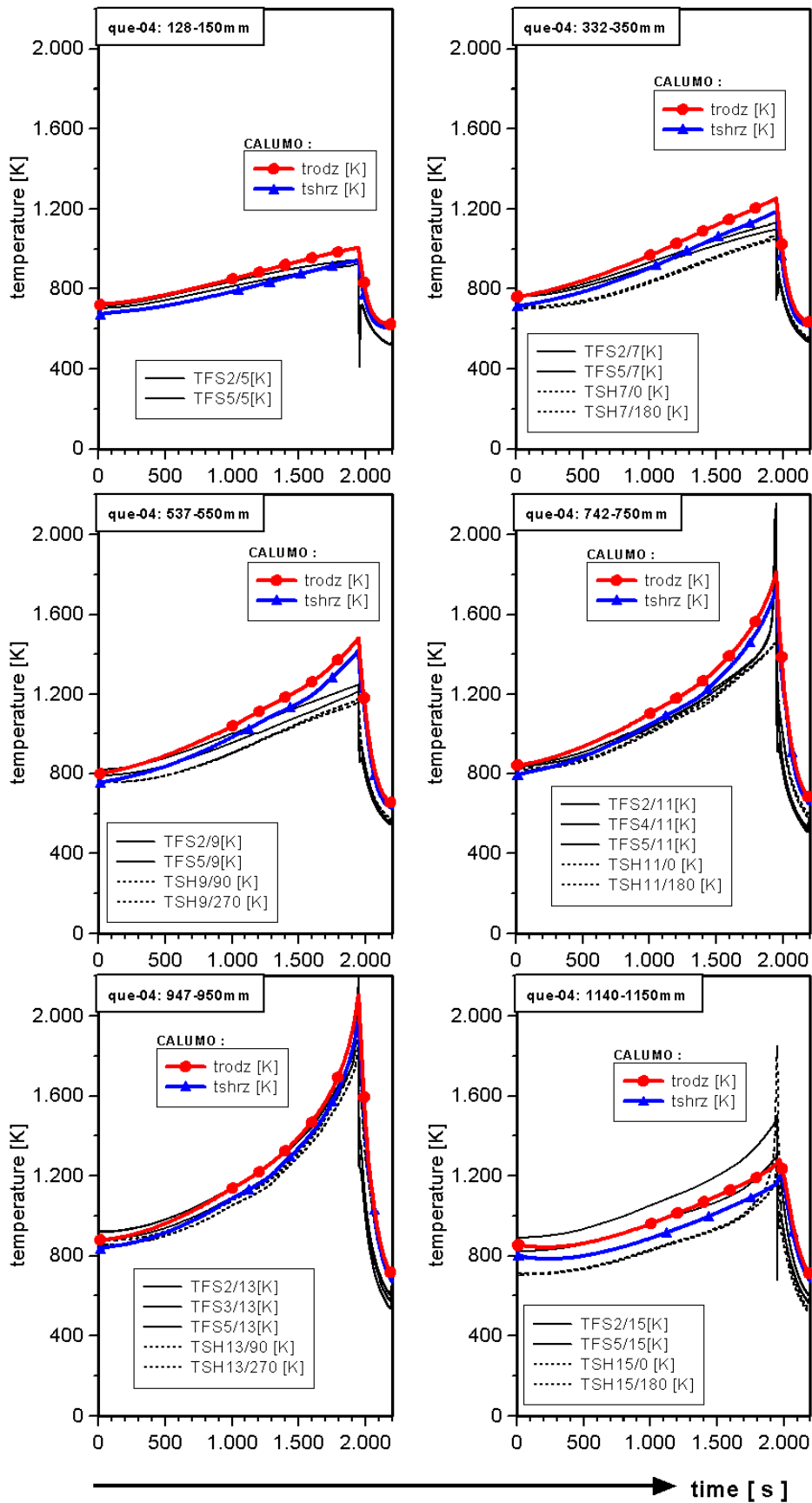
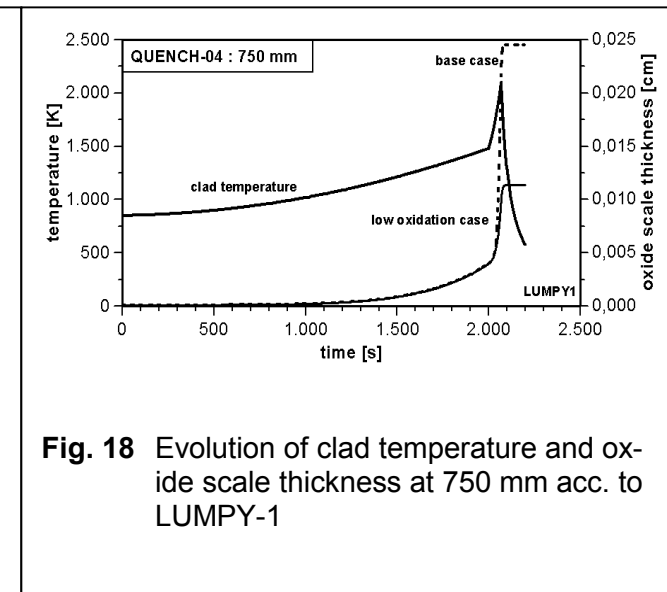
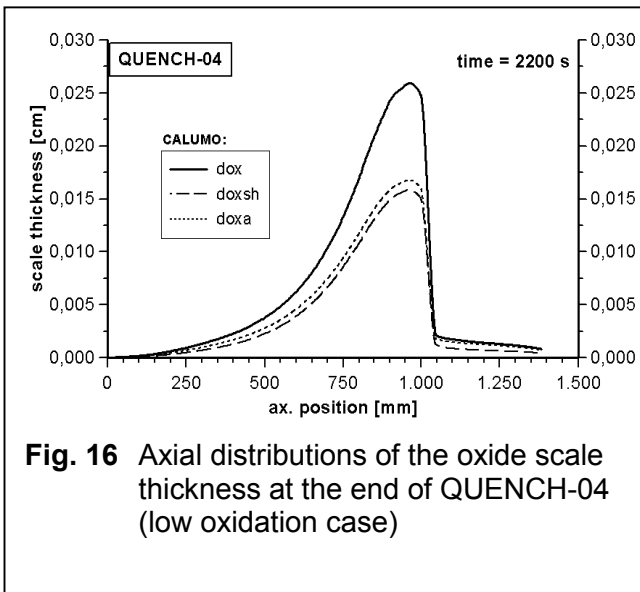
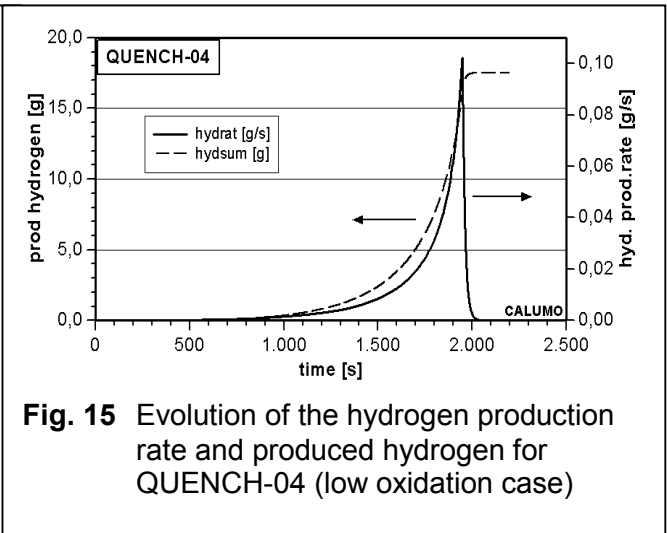
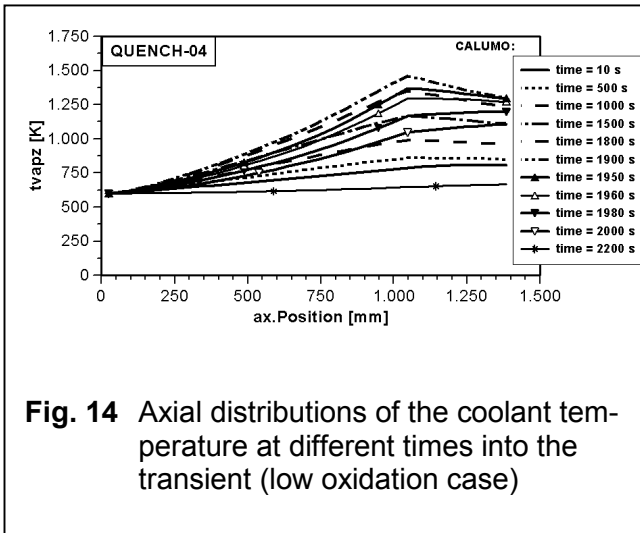
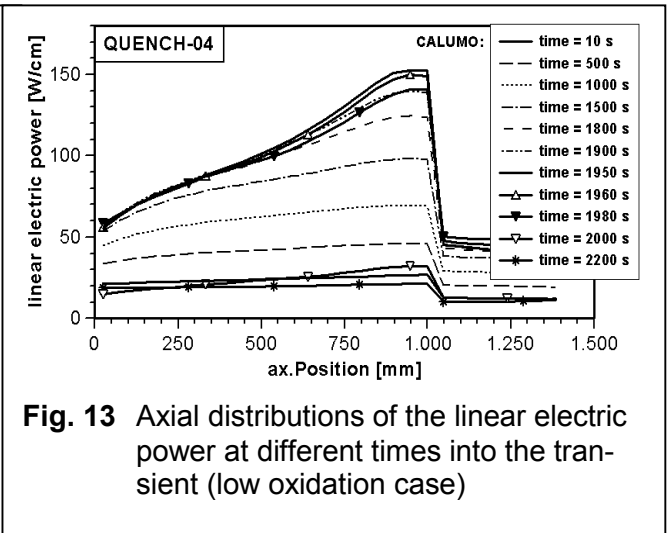
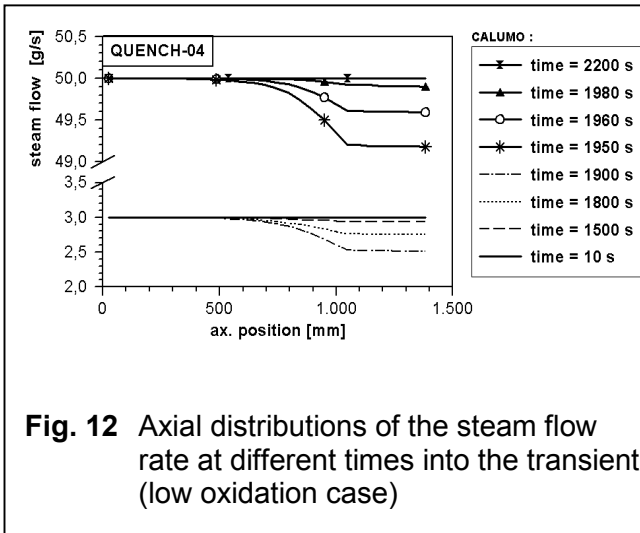


Fig. 11 Evolution of rod and shroud temperatures of QUENCH-04 at different axial locations (low oxidation case)



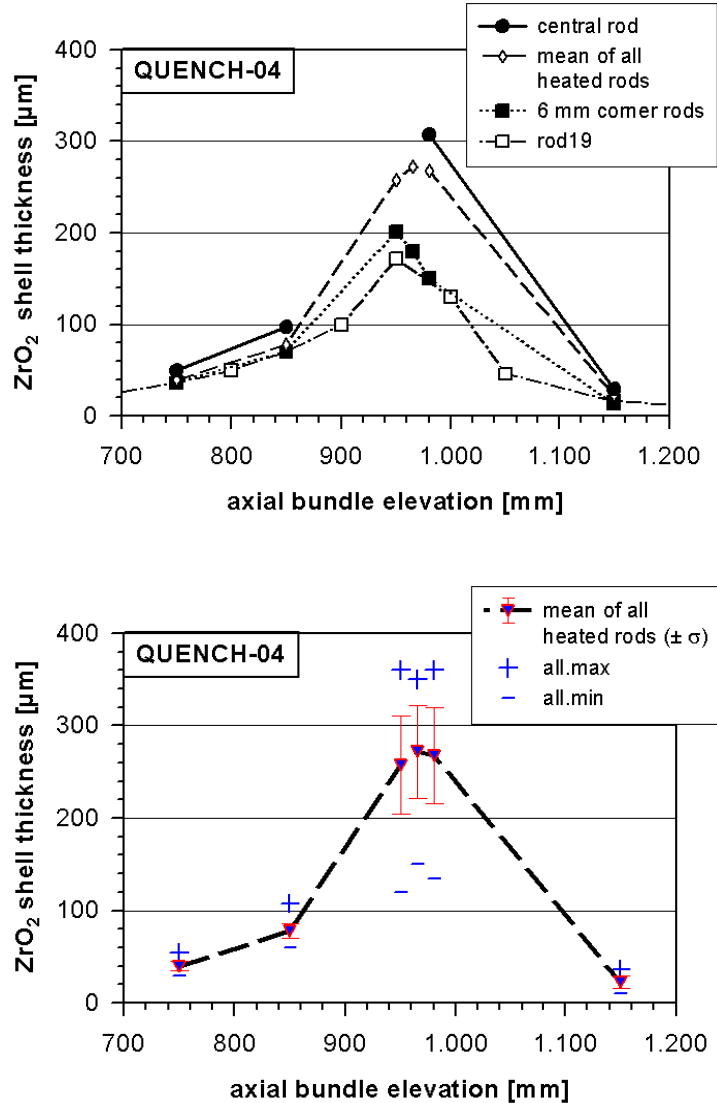


Fig. 17 Experimental values of oxide scales for the fuel rods of QUENCH-04 [13]

In QUENCH-03 the steam flow rate is reduced by about 50 % at the end of the transient phase and thus far from the steam starvation regime. The oxide scales in the high temperature region are between about 200 and 350 μm. The produced hydrogen at the end of the transient phase is about 18 g, somewhat below the value measured by the mass spectrometer (ca. 25 g). The maximum hydrogen production rate is about 0,15 g/s. If the steam flow would be completely consumed the hydrogen production rate would reach a value of 0,33 g/s. Thus, the results on the steam flow reduction in Fig. 5 is consistent with the calculated hydrogen production rate.

For QUENCH-04 the agreement between measured and calculated temperatures is not as good as with QUENCH-03. For axial locations below about 750 mm the calculated temperature increase rates are too high from about 1000 s into the transient. It is at the moment not clear why we have found a rather good for QUENCH-03 and a poorer one in QUENCH-04. During the QUENCH-03 test the test section had been severely damaged and parts of it had to renewed, especially the shroud and the isolation. It may be that the heat losses in QUENCH-04 are indeed higher than in QUENCH-03. But we have not yet tried to do sensitivity studies on the heat losses and do not know whether an increase within reasonable limits might explain the discrepancies. Also the very steep temperature escalation at 750 mm

towards the end of the transient phase is not reproduced by the code. It is not known whether this temperature escalation has the same cause as in QUENCH-03. For 950 mm the agreement is rather good, whereas in the upper part (1150 mm) the calculated temperatures are a bit too low. As with QUENCH-03 the temperature escalation in the upper part of the shroud is not reproduced by the code. We hold that the reason for this temperature escalation is the same as for QUENCH-03.

The maximum hydrogen production rate, as calculated by the code is nearly 0,1 g/s (see Fig. 15) and the overall produced hydrogen about 18 g about 30 % higher than the experimental value (≈ 12 g). But one should not forget that the measured values concern the released hydrogen. Part of the hydrogen is retained in the metal phase. This fraction could certainly comprise some grams of hydrogen. The calculated maximum value of the hydrogen production rate is distinctly below the maximum value measured by the mass spectrometer (0,3-0,4 g/s). There might be a QUENCH effect, which is not yet modeled in the code, for example crack formation in the oxide scales. But the measured hydrogen production rates should be also taken with caution.

A very important result of the code concerns Fig. 16, the oxide scales thickness of the fuel rods (dox = oxide scales of the inner clusters, doxa = oxide scales of the outer row) and the shroud (doxsh). At 2200 s into the transient the temperatures are already rather low and the calculated axial distributions are representative for the end of life state and can therefore be compared to the findings of PTE (see Fig. 17). Fortunately, in QUENCH-04 the fuel rods and the shroud remained fairly intact and a comparison between measured and calculated values is possible.

The experimental values at different cross sections scatter considerably, due to azimuthal and radial temperature differences. The higher the temperature reached at a certain axial position, the higher are the temperature differences. Thus, at 950 mm the scatter of experimental values is rather high (110-355 μm). If one disregards the corner rods the spread of data is a bit smaller (185-355 μm).

The overall features of the experimental values is reproduced by the code, although in details there are considerably discrepancies. The maximum calculated oxide scale thickness is distinctly lower (260 μm) than the value determined by PTE (350 μm).

At 750 and 850 mm the calculated values are too high. But as important temperature escalations have been detected by the instrumentation at these axial positions, the measured values of the oxide scales seem rather low.

Thus, for 750 mm the measured temperature curve has been given as input into the code LUMPY1. This code is able to calculate the evolution of the oxide scale based on a known temperature evolution, using experimental correlations for the oxidation. We have done this calculation for the base case and the low oxidation case (see Fig. 18). For the base case we would obtain a value of nearly 250 μm and for the low oxidation case a value of about 115 μm for the oxide scale at the end of the test. This is considerably higher than the experimental values (about 50 μm).

There occurred some axial relocation of the bundle after the test. But this was taken into account at cutting and we do not believe that this is the reason for the discrepancy as it appears also at 850 mm, although less severe.

But the question is whether correlations obtained from steady-state conditions can be applied without modification under transient conditions. It seems that with slow transients there is no problem but with steep transients as at 750 mm there is. It looks as if the temperature escalation has no impact on the oxidation rates. If one would have kept the low temperature increase rates one would have calculated a value of about 50 μm in accord with the experimental findings.

It appears that the sensitivity of the oxidation rates on temperature escalations depends on the temperature which has been reached before the escalation. If the temperature is already sufficiently high, the temperature escalation has an impact and steady-state correlations can

be applied. The question about the applicability of steady-state oxidation correlations under transient conditions is a generic issue. It might explain why we have obtained so poor an agreement for the base case calculations.

Mechanical effects are not yet modelled in the CALUMO code. Up to now we have found no strong indications for them, with the sole exception of bending effects and their consequences on radial heat transfer. In the transient phase of QUENCH-03 mechanical effects probably do not play a role. In the quench phase of QUENCH-04 they should have some impact. But there are other ill-understood effects like transient oxidation, which overshadow the impact of mechanical effects.

8. Conclusion

The calculations with CALUMO for QUENCH-03 and QUENCH-04 provided rather encouraging results. Of course, two tests do not suffice to validate a code, all the more as there are some serious discrepancies with the experimental results.

From the view point of modeling the FZK QUENCH tests are characterized by a coupling of the thermohydraulic conditions of the test section and the transient oxidation kinetics of the Zircaloy eventually disturbed by mechanical effects especially during quenching. In both domains serious questions arise. The most important ones concern the convective regime in the Ar volume around the upper part of the shroud and its eventual impact on the heat losses in the heated part and the application of steady-state oxidation correlations under transient conditions.

References

- [1] S. Hagen, et al.: Essential results of the CORA program; 3rd International QUENCH-Workshop, FZK, December 1997.
- [2] W. Hering, et al.: Untersuchungen zur Kernzerstörung; Beitrag zu FZK-Nachrichten 4/97, S. 309-325 (1997).
- [3] W. A. Sutherland: Heat transfer to superheated steam; GEAP-4258 (1963).
- [4] C. R. Wilke: J. Chem. Phys. 18 (1950), p. 517.
- [5] M. Moalam and D. R. Olander: Oxidation of Zircaloy by steam; Journal Nuclear Materials 182 (1990), pp. 170-194.
- [6] R. Zurmühl: Praktische Mathematik, Springer Verlag Berlin/Heidelberg/New York (1965), pp. 417-420.
- [7] P. Hofmann, et al.: QUENCH-01 – Experimental and Computational Results; FZKA 6100 (1998).
- [8] S. Leistikow, et al.: Kinetik und Morphologie der isothermen Dampfoxidation von Zircaloy-4 bei 700 bis 1300 °C; KFK 2587 (1978).
- [9] P. Hofmann, et al.: Physico-chemical Behaviour of Zircaloy Fuel Rod Cladding Tubes During LWR Severe Accident Reflood; FZKA 5846 (1997).
- [10] J. T. Prater, E. L. Courtright: Zircaloy-4 Oxidation at 1300 to 2400 °C; NUREG/CR-4889 (1987).
- [11] P. Hofmann, et al.: Experimental and Computational Results of the Experiments QUENCH-02 and QUENCH-03, FZKA 6295 (2000)
- [12] L. Sepold, et al.: QUENCH-04 Test Data Report, Interner Bericht 421/99, PSP 3327 (1999).
- [13] U. Stegmaier: Personal Communication.
- [14] G. Choi and S. A. Korpela: Stability of the Conduction Regime of Natural Convection in a Tall Vertical Annulus; J. Fluid Mech. 99 (1980), pp. 725-738.

Annex I

Dateral data correlations

cpw(tk)	=	0.1343+0.1894e-4*(tk-273.)
at(tk)	=	0.28*EXP(-10103./tk)
cpst(tk)	=	1.683+0611e-3*tk
wiso(tk)	=	6.0e-4+2.207e-7*(tk-273.)+5.06e-10*(tk-273.)**2
rhoar(pres, tk)	=	pres*0.481/tk
rhost(pres, tk)	=	pres*0.2164/tk
wlmo(tk)	=	1.37-2.36e-4*tk
wlwo(tk)	=	0.601+2.39e-4*tk
wlcu(tk)	=	3.91-8.5e-4*(tk-273.)
rhoW(tk)	=	2.61e-6+2.63e-8*tk+2.2e-12*tk**2
rhoM(tk)	=	2.29e-6+5.36e-9*tk+1.38e-11*tk**2-2.22e-15*tk**3
rhoC(tk)	=	7.89e-7+9.9e-9*tk-5.49e-12*tk**2+3.16e-15*tk**3
aht(tk)	=	5.46*EXP(-14210./tk)
cpmo(tk)	=	0.255+0.514e-4*(tk-273.)+0.455e-8*(tk-273.)**2
cpcu(tk)	=	0.387+0.872e-4*(tk-273.)
visar(tk)	=	2.1e-4+0.551e-6*(tk-273.)-1.46e-10*(tk-273.)**2
visst(tk)	=	0.8e-4+3.966e-7*(tk-273.)
wlar(tk)	=	2.23e-4+2.67e-7*(tk-273.)
wlst(tk)	=	1.82e-4+0.556e-6*(tk-273.)+8.4e-10*(tk-273.)**2
CPAR	=	0.502
FLUOX	=	rate parameter for the oxygen flux ($j^{ox} = \frac{FLUOX}{\delta^{ox}}$)
AT	=	rate parameter for oxide scale thickness according to [8] $(\delta^{ox} = AT(TK)\sqrt{t})$
ATH	=	rate parameter for oxide scale thickness according to [10] $(\delta^{ox} = ATH(TK)\sqrt{t})$
CPW	=	specific heat capacity of Tungsten
CPST	=	specific heat capacity of steam
CPMO	=	specific heat capacity of Molybdenum
CPCU	=	specific heat capacity of Copper
CPAR	=	specific heat capacity of Argon
CPC1	=	specific heat capacity of Zircaloy
CPC2	=	specific heat capacity of ZrO ₂

WISO	=	heat conductivity of Zirconia insulation
WLAR	=	heat conductivity of Argon
WLST	=	heat conductivity of steam
WLMO	=	heat conductivity of Molybdenum
WLWO	=	heat conductivity of Tungsten
WLCU	=	heat conductivity of Copper
CWH1	=	heat conductivity of Zircaloy
CWH2	=	heat conductivity of ZrO ₂
RHOW	=	specific electric resistance of Tungsten
RHOC	=	specific electric resistance of Copper
RHOM	=	specific electric resistance of Molybdenum
VISSAR	=	dyn. viscosity of Argon
VISST	=	dyn. viscosity of steam
RHOAR	=	spec. density of Argon
RHOST	=	spec. density of steam

```

Function CPC1 (TKELV)
Spezifische Wärme von Zry in J/g/K
if (TKELV.GE.1248.) then CPC1=356.
else
if (TKELV.LE.1083.) then CPC1=281.+0.11899*(TKELV-300.)
else
if (TKELV.LE.1173.) then CPC1=374.+4.9111*(TKELV-1.083.)
else
CPC1=816-6.13333*(TKELV-1173.)
endif
CPC1=CPC1*1.E-3
if (TKELV.GE.2098..AND.TKELV.LE.2125.) CPC1=CPC1+9.44
end

```

```

Function CPC2 (TKELV)
Spezifische Wärme von ZRO2 in J/g/K
if (TKELV.LT.1478.) then
CPC2=565.+6.11E-2*TKELV-1.14E7/TKELV**2
else
if (TKELV.LE.2000.) then
CPC2=604.5
else
CPC2=171.7+0.2164*TKELV
endif
CPC2=CPC2*1.E-3
if (TKELV.GE.2950..AND.TKELV.LE.3000) CPC2=CPC2+10.66
end

```

Function CWH1 (TKELV) Wärmeleitfähigkeit von ZRY in W/cm/K $CWH1=0.20457+1.2047E-4*TKELV-5.7368E-8*TKELV**2$ end
Function CWH2 (TKELV) Wärmeleitfähigkeit von ZRO2 in W/cm/K $CWH2=1.67+3.62E-4*TKELV$ ZRO2 on cladding $CWH2=CWH2*1.E-2$ end
Function FLUOX (TK) if (TK.LE.1783.) then VESHCHUNOV $FLUOX=0.0983*EXP(-20373./TK)$ else $FLUOX=31.34*EXP(-27430./TK)*0.5$ endif end

Annex II

Nomenclature

ρ	=	specific density
μ	=	dynamic viscosity
λ	=	thermal conductivity
v	=	velocity
M	=	molecular weight
u	=	circumference
r	=	specific electrical resistance
R	=	electrical resistance, general gas constant
η	=	mol fractions
v	=	moles
P	=	total power
χ	=	linear power
F	=	area, cross section
t	=	time
z	=	axial position
c_p	=	heat capacity
m	=	total linear mass
T	=	temperature
w	=	linear power or heat flux
δ	=	thickness
j	=	flux

Superscripts and subscripts

b	=	bundle
cl	=	cladding
ox	=	oxide
y	=	Zircaloy
el	=	electric or electrode
rad	=	radiation
cool	=	coolant
st	=	steam
rod	=	fuel rod simulator
sh	=	shroud

i	=	inner
o	=	outer
W	=	tungsten
Mo	=	molybdenum
Cu	=	copper
u	=	upper
l	=	lower
in	=	inlet
out	=	outlet
cj	=	cooling jacket